Electronic Supplementary Material (ESI) for ChemComm.

Supporting Information for

2D Salphen-based heteropore covalent organic frameworks for highly efficient electrocatalytic water oxidation

Lin-Lin Wang,[a] Wen-Da Zhang,[a] Tao Li,[a] Xiaodong Yan,[a] Jie Gao,[a] Yu-Xuan Chen,[a] Ya-Xiang Shi,[a] Zhi-Guo Gu[*a,b]

[a] Key Laboratory of Synthetic and Biological Colloids, Ministry of Education, School of Chemical and Material Engineering, Jiangnan University, Wuxi 214122, China.

[b] International Joint Research Center for Photoresponsive Molecules and Materials, School of Chemical and Material Engineering, Jiangnan University, Wuxi 214122, China.

E-mail: zhiguogu@jiangnan.edu.cn

1. General Information

All chemicals were reagent grade, purchased from commercial sources and used without further purification. Fourier transform infrared (FT-IR) measurements were performed on a Thermo Nicolet iS10 spectrometer in the range of 500-4000 cm^{-1}. ^{13}C cross-polarization with magic angle-spinning (CP-MAS) solid-state nuclear magnetic resonance (NMR) spectra were recorded on a Bruker ARX 300 MHz spectrometer. X-ray photoelectron spectroscopy (XPS) analysis was measured by a Kratos Axis Supra instrument using a monochromatized Al Ka radiation as X-ray source. Thermogravimetric analyses (TGA) were obtained using a Mettler Toledo TGA/DSC1/1100SF analyser in the temperature range of 30 to 800 °C under flowing N_2. The Brunauer-Emmett-Teller (BET) surface area was evaluated by N_2 sorption isotherms collected at 77 K using a Micromeritics ASAP2020 surface area and pore size analyser. Pore size distribution was determined by nonlocal density functional theory mode in the instrument software package. Scanning electron microscopy (SEM) images were obtained on a Hitachi S-4800. Transmission electron microscopy (TEM) images were obtained on a JEOL JEM-2100. HRTEM images and EDS mapping were carried out on a Tecnai G2 F30 transmission electron microscopy at an acceleration voltage of 300 kV. Powder X-ray diffraction (PXRD) patterns were collected on a D8 Advance X-ray diffractometer (Bruker AXS Germany) with Cu Kα radiation at 40 kV 200 mA with scanning rate of $2°\cdot min^{-1}$ (2θ) at room temperature.

2. Electrochemical performance experiments

The electrochemical performances of the samples were evaluated on an electrochemical working station (CHI760E). Cyclic voltammetry (CV) and electrochemical impedance spectroscopy (EIS) measurements were conducted on in a three-electrode setup, using a Pt plate (1 cm^2) as the counter electrode and Hg/HgO electrode as the reference electrode. The working electrode was prepared as follows. Typically, 5 mg of the electrocatalyst powder was dispersed in 0.96 mL of 1:1 (V/V) deionized water/EtOH mix solvent with 40 μL of Nafion solution. The mixture was sonicated for about 1 h to form a homogeneous catalyst ink. 160 μL of the catalyst ink was coated on the Ni foam and dried in oven for 12 h. The mass loading on each electrode is about 0.80 mg cm^{-2}. All the electrochemical measurements were recorded in 1 M KOH aqueous electrolyte. EIS spectra were collected at 1.52 V versus RHE in the frequency range from 0.01 to 10^5 Hz with a amplitude of 5 mV. Before collecting the data, the catalyst electrodes were run for 10 cycles for activation. Linear sweep voltammogram (LSV) was obtained at the scan rate of 10 mV s^{-1} in 1 M KOH. Tafel slopes were derived from the LSV curves. Chronopotentiometric measurements were conducted for the stability test at a current density of 10 mA cm^{-2} for 10 h. The potential was converted according to the equation: $E_{RHE} = E_{Hg/Hgo} + 0.098 + 0.059 \times pH = E_{Hg/Hgo} + 0.924$. The overpotential was computed as: $\eta = E_{RHE} - 1.23$ V.

3. Experimental section

Synthesis of **Salphen-COF**

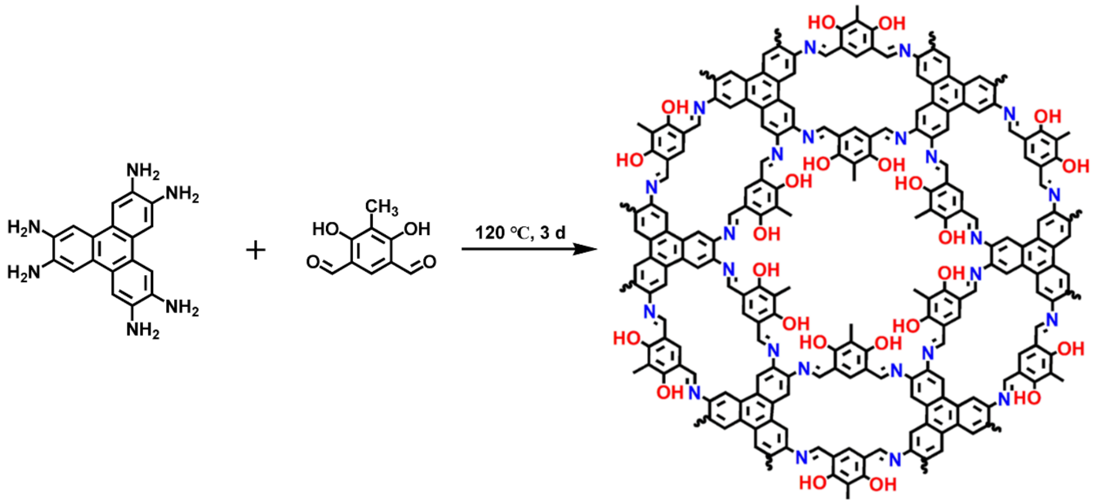

Triethylamine (Et_3N) (25%, 100 μL) was added to a solution of 12.62 mg of HATP·6HCl in 5 mL of water, after sonicating for 2 minutes, centrifuge to collect the precipitate for use. Add 0.286 mL of mesitylene and 1.714 mL of 1,4-dioxane to the above precipitation and transfer to a glass bottle (volume of ca. 10 mL), then add 4,6-Dihydroxy-5-methyl-1,3-diformyl benzene (DMDB) (12.7 mg, 0.105 mmol) to the glass bottle. The resulting solution was sonicated for 10 minutes to obtain a homogenous dispersion, to which 0.2 mL of 6 M aqueous acetic acid (AcOH) was added. The glass bottle was transferred into a 25 mL Teflon-lined stainless steel autoclave. The autoclave was sealed and heated at 120 °C for 3 days and then cooled to room temperature. The formed brown precipitate was collected by filtration and washed with ethanol (3 × 20 mL), DMF (3 × 20 mL) and acetone (3 × 20 mL), soxhlet extracted by THF 24 h, then dried at 120 °C under vacuum for 24 h to give a brown powder with 81% yield. FT-IR (powder): ν_{max} 1620, 1510, 1419, 1374, 1316, 1298, 1223, 1160, 1069, 1001, 884, 799, 718 and 655 cm^{-1}.

Synthesis of **Ni-Salphen-COF**

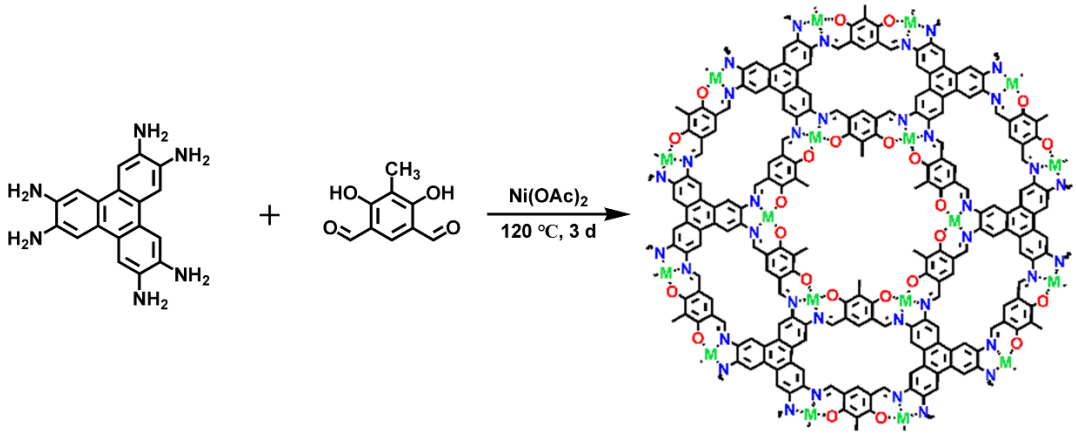

Triethylamine (Et_3N) (25%, 100 μL) was added to a solution of 12.62 mg of HATP·6HCl in 5 mL of water, after sonicating for 2 minutes, centrifuge to collect the precipitate for use. Add 0.286 mL of mesitylene and 1.714 mL of 1,4-dioxane to the above precipitation and transfer to a glass bottle (volume of ca. 10 mL), then add 4,6-Dihydroxy-5-methyl-1,3-diformyl benzene (DMDB) (12.7 mg, 0.105 mmol) and excess $Ni(OAc)_2·4H_2O$ (20 mg, 0.080 mmol) to the glass bottle. The resulting solution was sonicated for 10 minutes to obtain a homogenous dispersion, to which 0.2 mL of 6 M aqueous acetic acid (AcOH) was added. The glass bottle was transferred into a 25 mL Teflon-lined stainless steel autoclave. The autoclave was sealed and heated at 120 °C for 3 days and then cooled to room temperature. The formed black precipitate was collected by filtration and washed with ethanol (3 × 20 mL), DMF (3 × 20 mL) and acetone (3 × 20 mL), soxhlet extracted by THF 24 h, and then dried at 120 °C under vacuum for 24 h to give a reddish brown powder with 75% yield. FT-IR (powder): ν_{max} 2921, 1621, 1582, 1523, 1487, 1428, 1379, 1267, 1158, 1114, 1015, 884, 849, 727 and 664 cm^{-1}.

Synthesis of **NiFe-Salphen-COF**

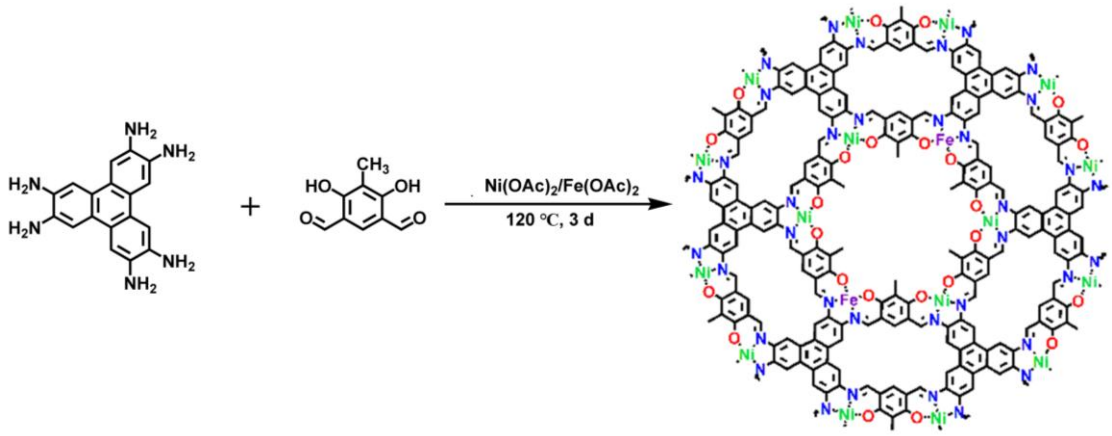

Triethylamine (Et_3N) (25%, 100 μL) was added to a solution of 12.62 mg (0.035 mmol) of HATP·6HCl in 5 mL of water, after sonicating for 2 minutes, centrifuge to collect the precipitate for use. Add 0.286 mL of mesitylene and 1.714 mL of 1,4-dioxane to the above precipitation and transfer to a glass bottle (volume of ca. 10 mL), then add 4,6-Dihydroxy-5-methyl-1,3-diformyl benzene (DMDB) (12.7 mg, 0.105 mmol) and $Ni(OAc)_2·4H_2O$ (18 mg, 0.072 mmol) and $Fe(OAc)_2$ (2 mg, 0.0172 mmol) to the glass bottle. The resulting solution was sonicated for 10 minutes to obtain a homogenous dispersion, to which 0.2 mL of 6 M aqueous acetic acid (AcOH) was added. The glass bottle was transferred into a 25 mL Teflon-lined stainless steel autoclave. The autoclave was sealed and heated at 120 °C for 3 days and then cooled to room temperature. The formed black precipitate was collected by filtration and washed with ethanol (3 × 20 mL), DMF (3 × 20 mL) and acetone (3 × 20 mL), soxhlet extracted by THF 24 h, then dried at 120 °C under vacuum for 24 h to give a reddish brown powder with 84% yield. FT-IR (powder): ν_{max} 2921, 1620, 1577, 1523, 1483, 1433, 1388, 1267, 1164, 1100, 886, 851, 727 and 662 cm^{-1}.

Note that we have prepared a series of **NiFe-Salphen-COFs** with different Ni/Fe ratios. The crystallinity and OER performance of the other **NiFe-Salphen-COFs** is not as good as those of **NiFe-Salphen-COF** with a Ni/Fe ratio of 4.2.

4. Characterization

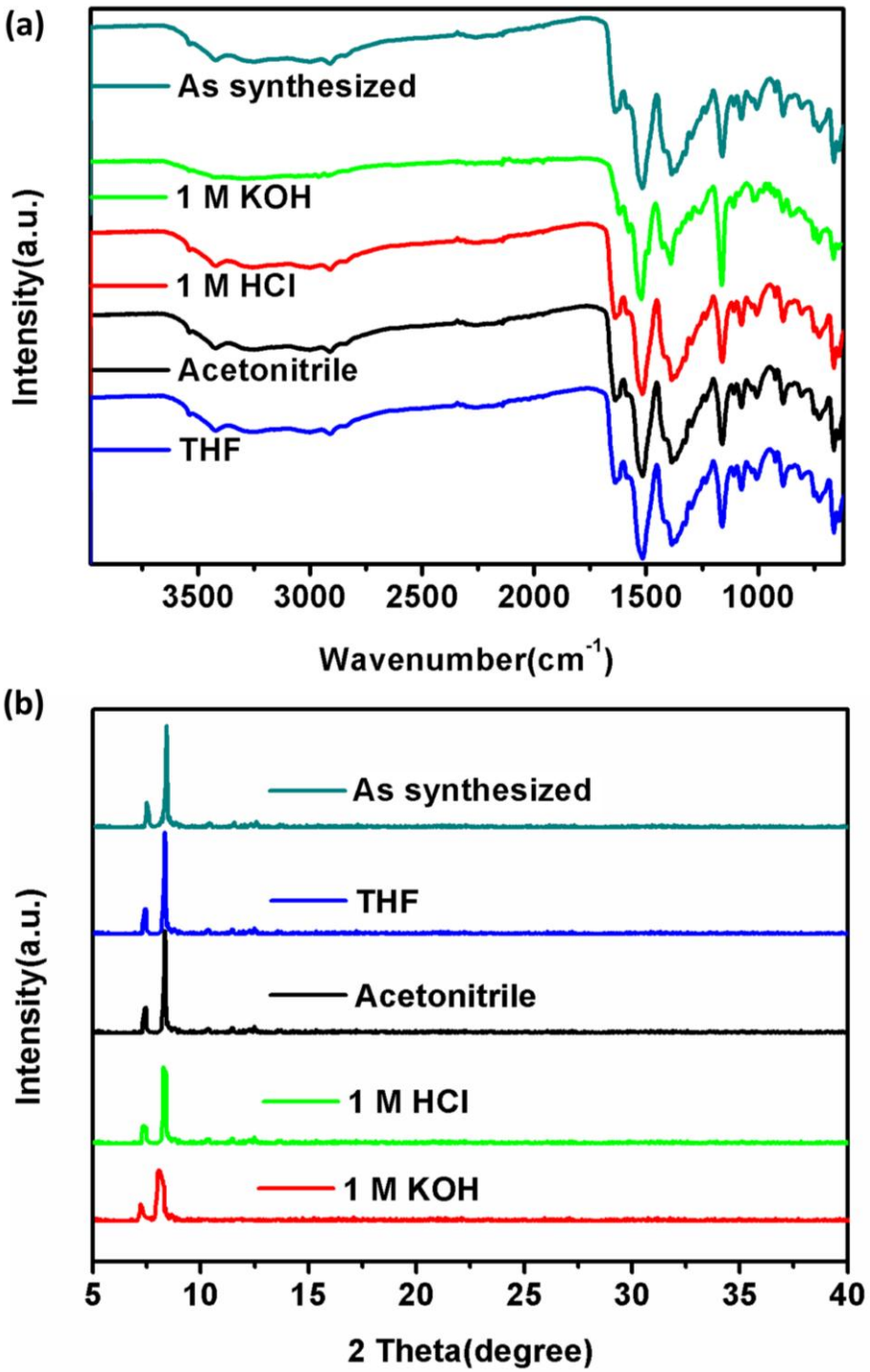

Fig. S1 (a) The FT-IR spectra and (b) PXRD patterns of **Salphen-COF** after treated in 1 M HCl, 1 M KOH and organic solvents.

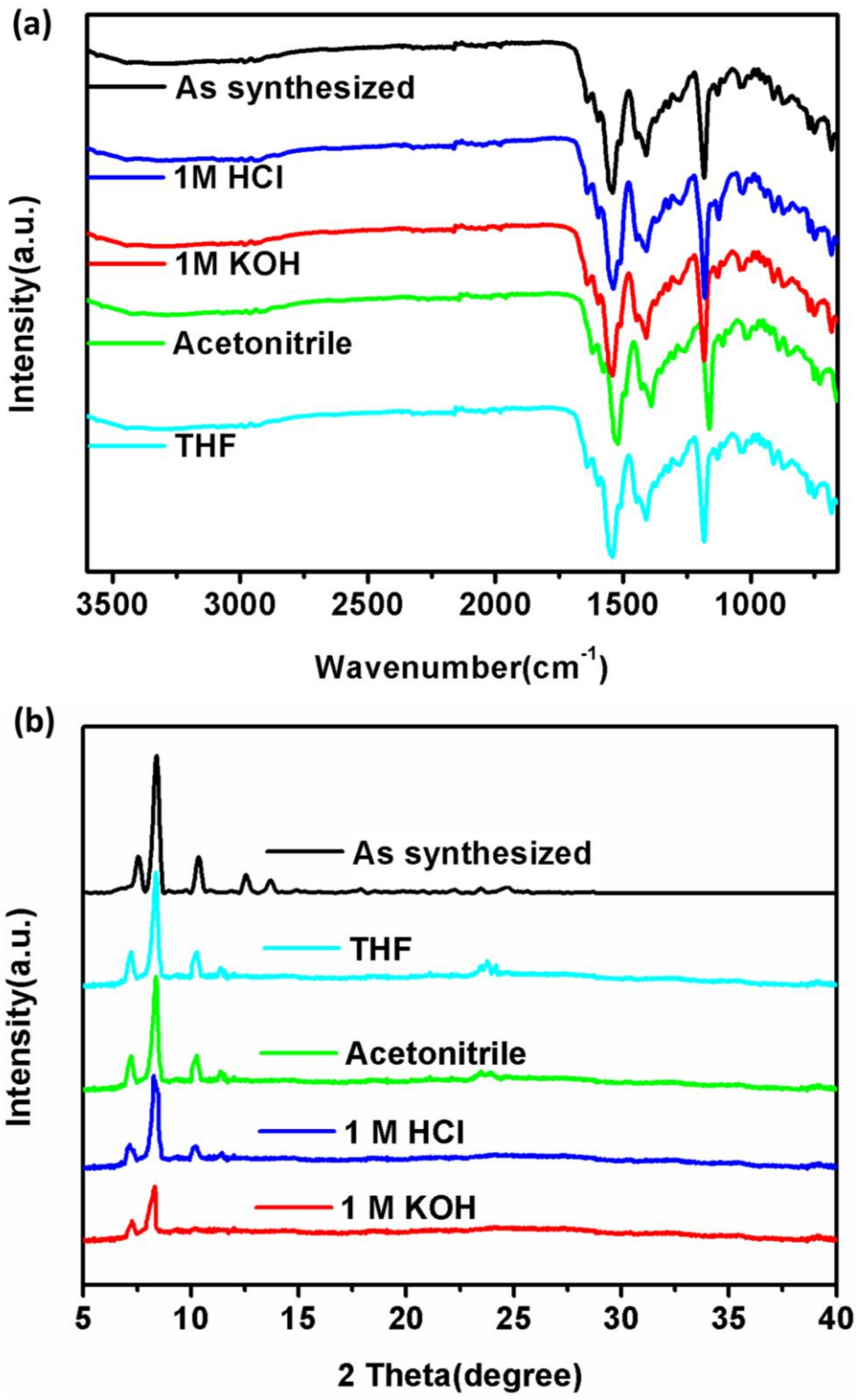

Fig. S2 (a) FT-IR spectra and (b) PXRD patterns of **Ni-Salphen-COF** after treated in 1 M HCl, 1 M KOH and organic solvents for 3 days.

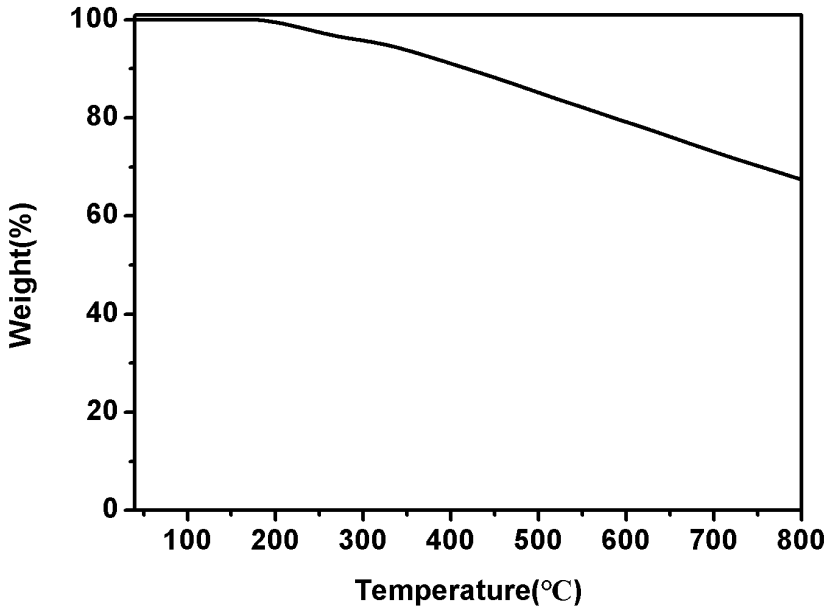

Fig. S3 Thermogravimetric analysis (TGA) curve of **Salphen-COF**.

Salphen-COF exhibited no discernible weight loss from 0 to 272 °C, and then started to decompose. At 800 °C, there was still 60% of weight residual. These indicate its excellent thermal stability.

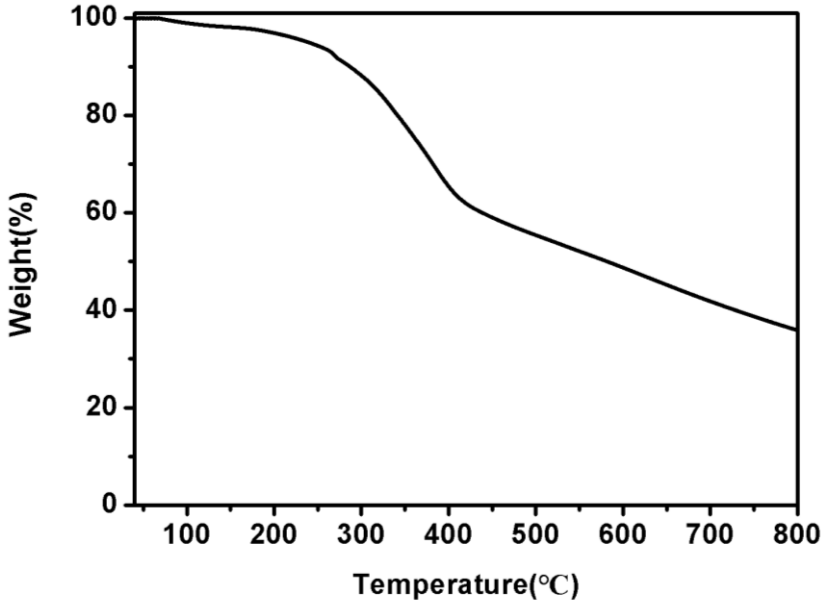

Fig. S4 Thermogravimetric analysis (TGA) curve of **Ni-Salphen-COF**.

Ni-Salphen-COF exhibited no discernible weight loss from 0 to 260 °C, and then started to decompose. At 800 °C, there was still 38% of weight residual. These indicate its high thermal stability.

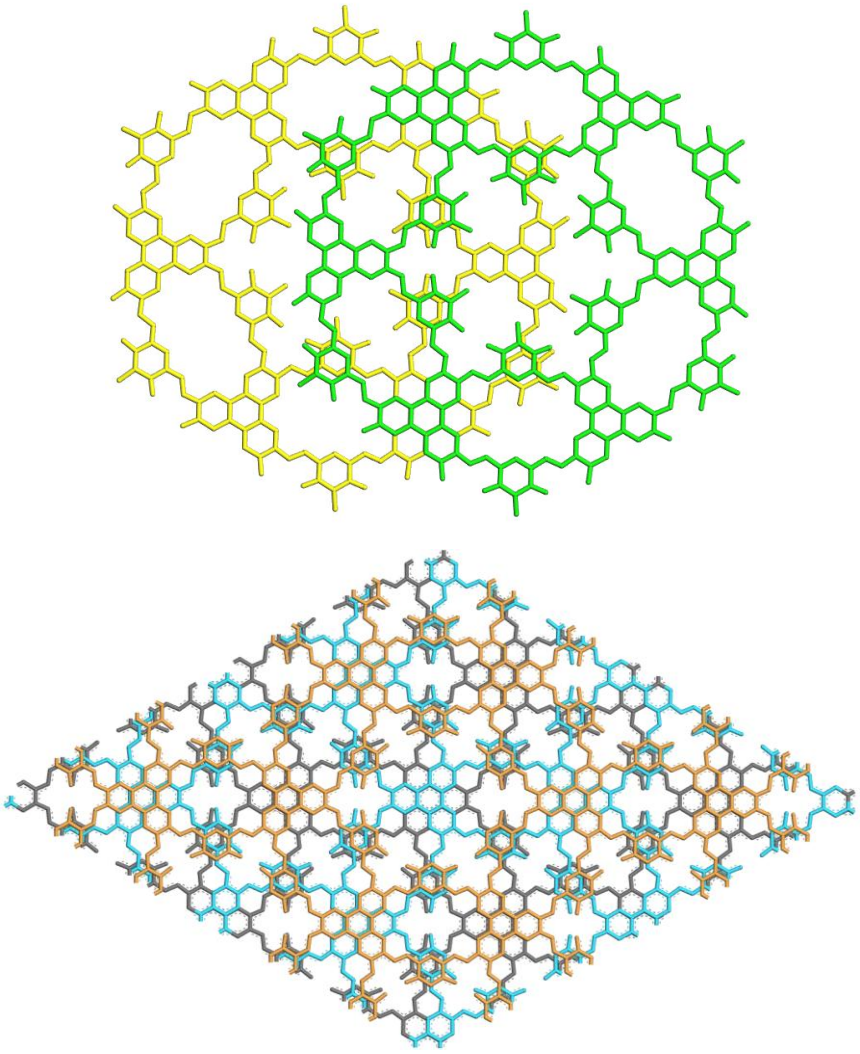

Fig. S5 Staggered AB stacking (top) and ABC stacking (down) of **Salphen-COF**.

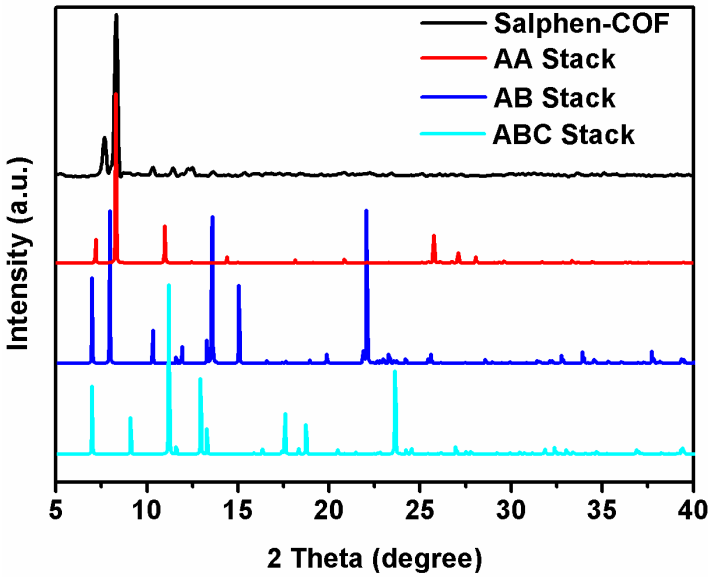

Fig. S6 Powder X-ray diffraction (PXRD) patterns of **Salphen-COF** (AA stacking, AB stacking and ABC stacking).

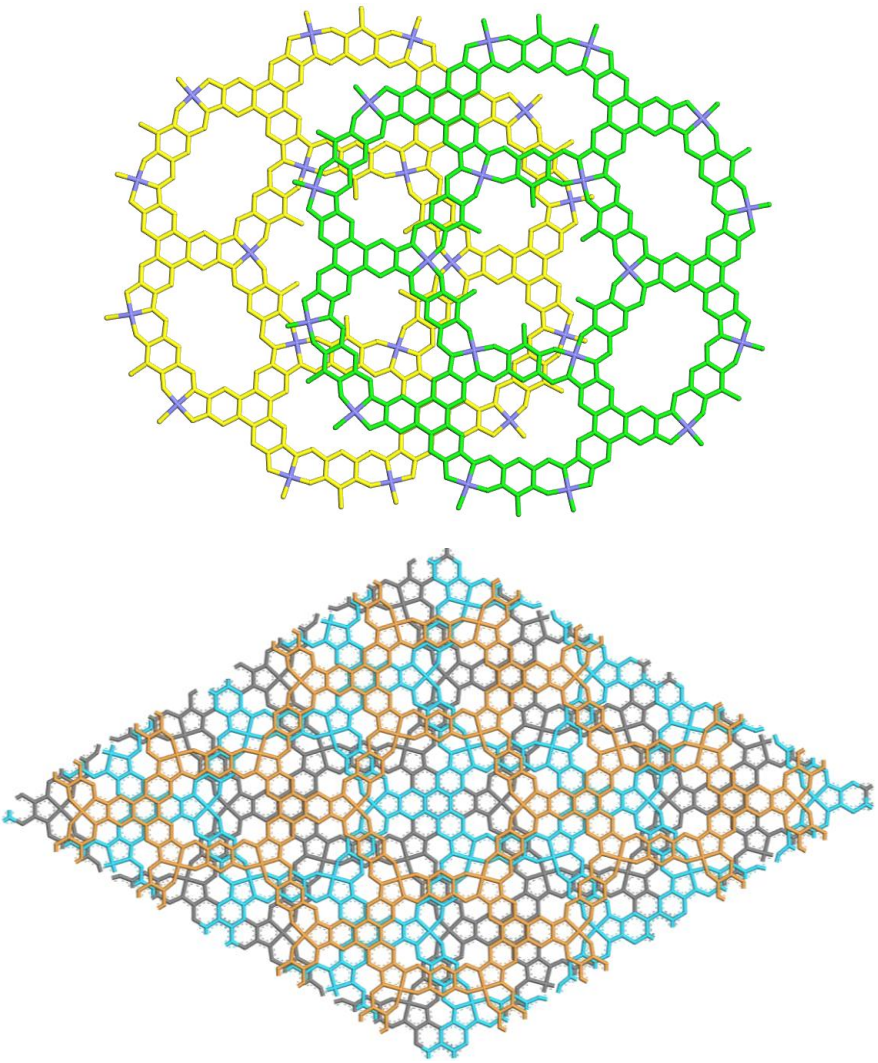

Fig. S7 Staggered AB stacking (top) and ABC stacking (down) of **Ni-Salphen-COF**

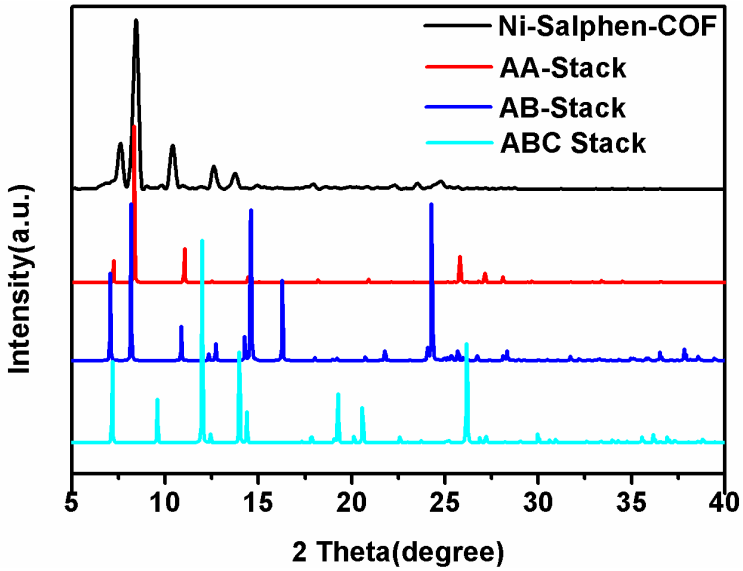

Fig. S8 Powder X-ray diffraction (PXRD) patterns of **Ni-Salphen-COF** (AA stacking, AB stacking and ABC stacking).

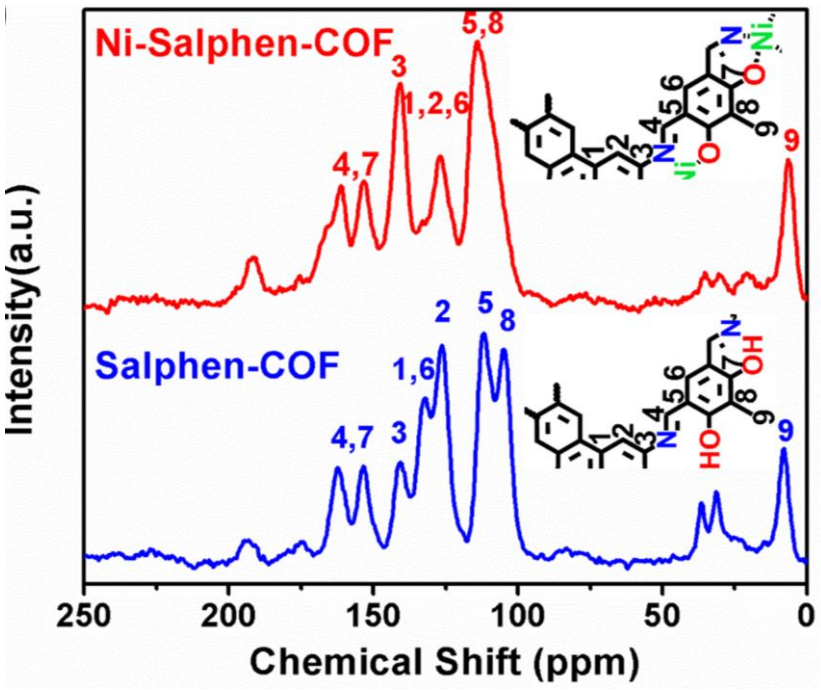

Fig. S9 Solid-state ^{13}C CP-MAS NMR spectrum of **Salphen-COF** and **Ni-Salphen-COF**.

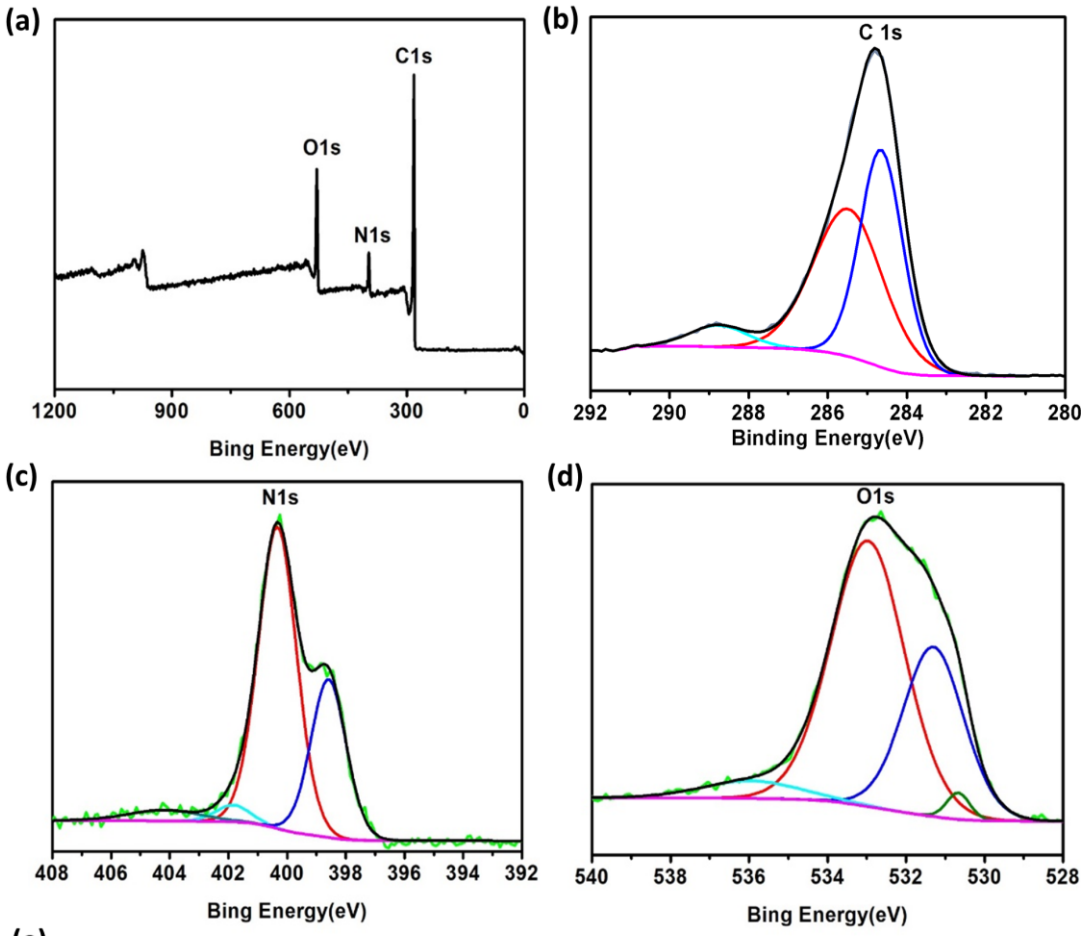

(e)

Elem.	Salphen-COF at.-%
C	78.01
N	7.54
O	14.45

at.-%: atomic ratio in percentage.

Fig. S10 XPS spectra of **Salphen-COF**. (a) Survey, (b) C 1s, (c) N 1s, (d) O 1s, (e) The elemental composition according to the XPS analysis.

The XPS survey of **Salphen-COF** confirms the presence of C, N and O. The signals at 401 and 533 eV correspond to N 1s and O 1s, respectively.

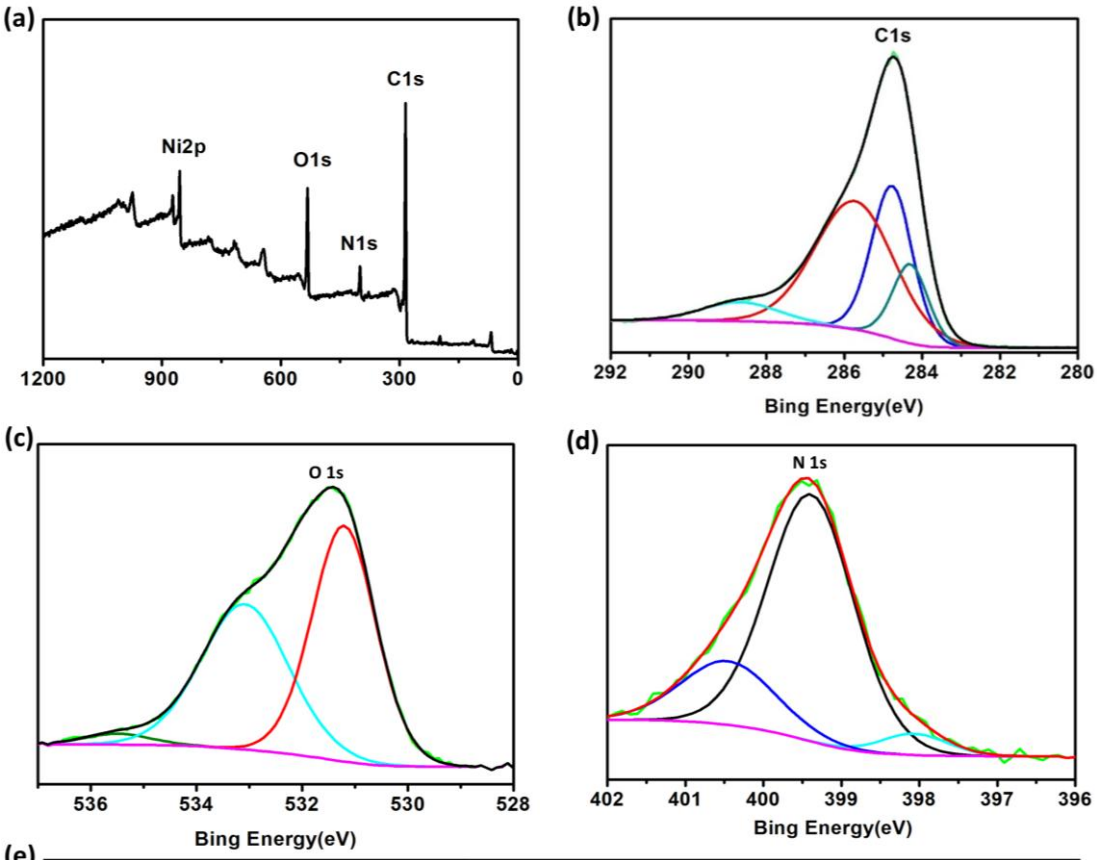

(e)

Elem.	Salphen-COF at.-%
C	75.80
N	6.14
O	15.08
Ni	2.98

at.-%: atomic ratio in percentage.

Fig. S11 (a) Survey, (b) C 1s, (c) O 1s and (d) N 1s spectra of **Ni-Salphen-COF**. (e) The elemental composition according to the XPS analysis.

The XPS survey of **Ni-Salphen-COF** confirms the presence of C, N, O and Ni. The signals at 399 and 534 eV correspond to N 1s and O 1s, respectively.

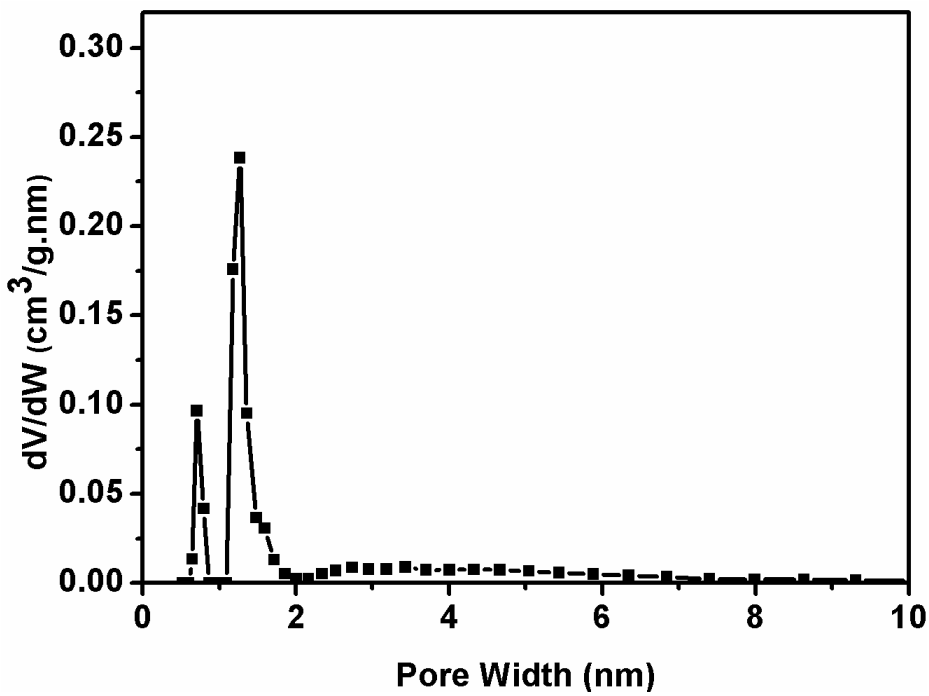

Fig. S12 Pore size distribution of **Salphen-COF**.

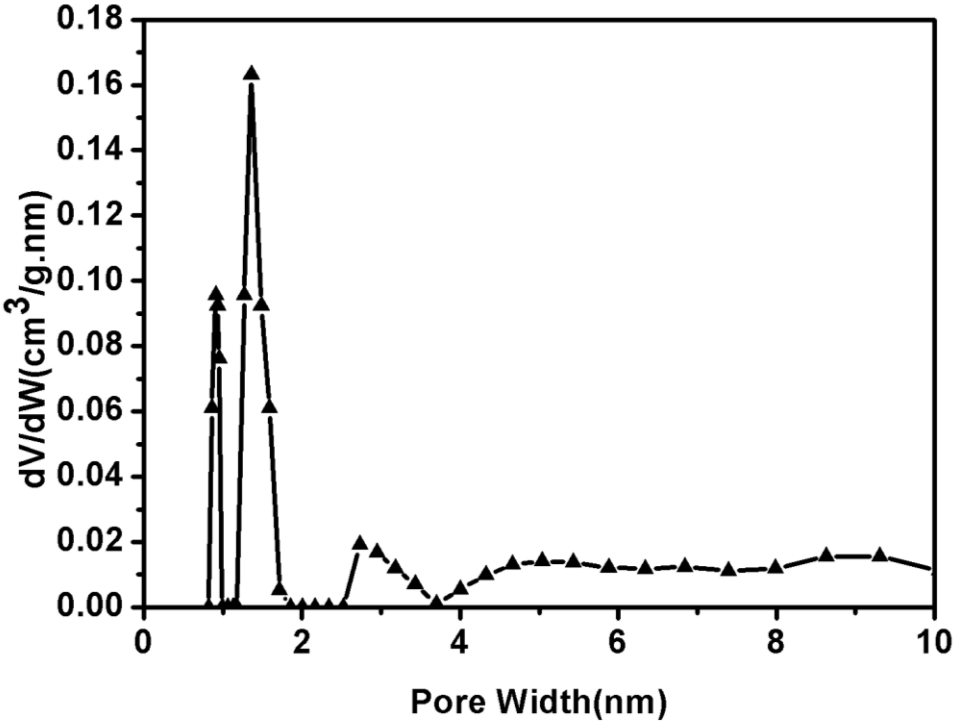

Fig. S13 Pore size distribution of **Ni-Salphen-COF**.

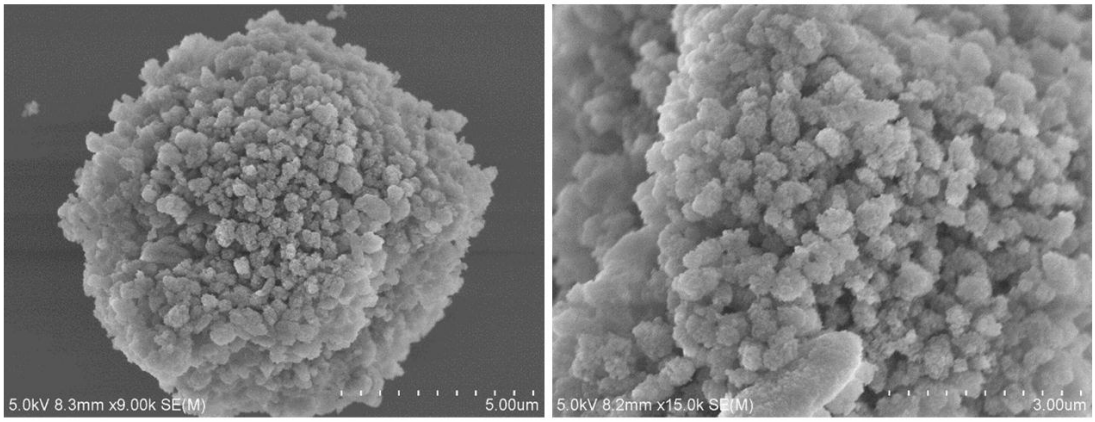

Fig. S14 SEM images of **Salphen-COF**.

SEM images show that **Salphen-COF** has a spherical shape composed of many nanoparticles.

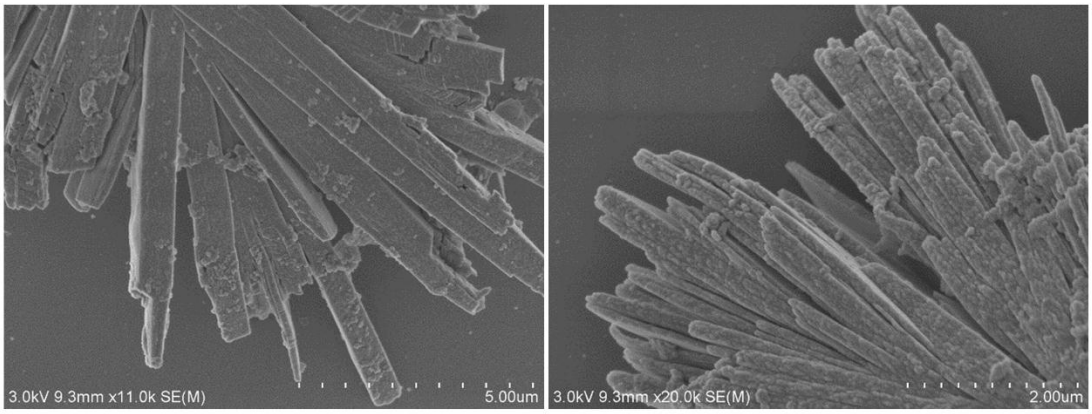

Fig. S15 SEM images of **Ni-Salphen-COF**.

Ni-Salphen-COF has a rod-like morphology likely comprised of nanosheets.

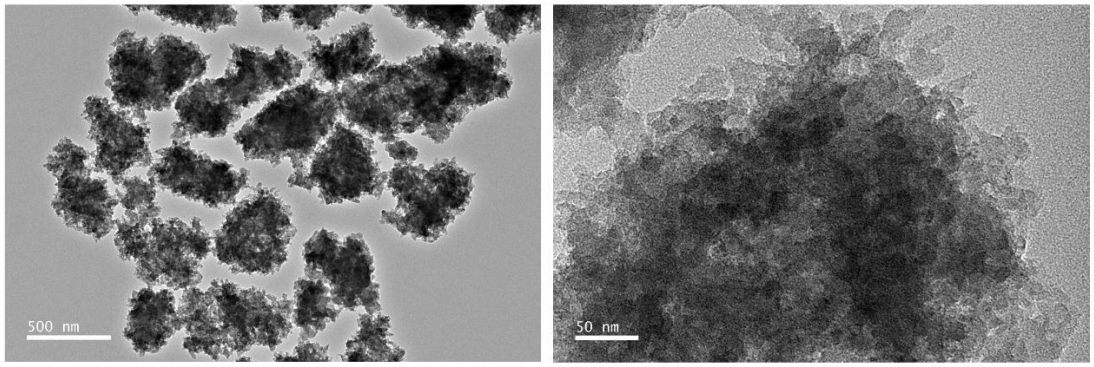

Fig. S16 TEM images of **Salphen-COF**.

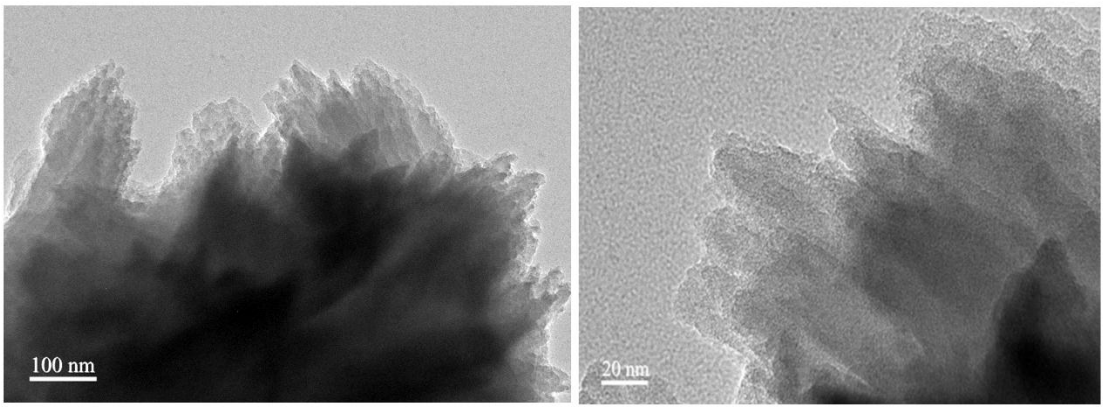

Fig. S17 TEM images of **Ni-Salphen-COF**.

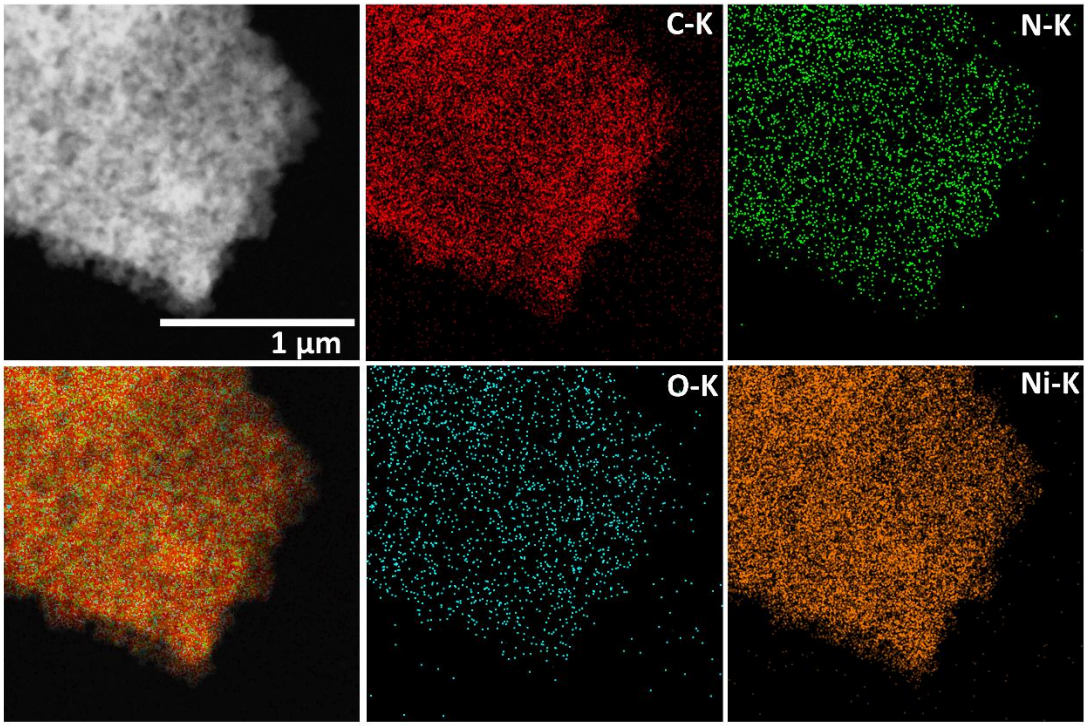

Fig. S18 Mapping of **Ni-Salphen-COF**.

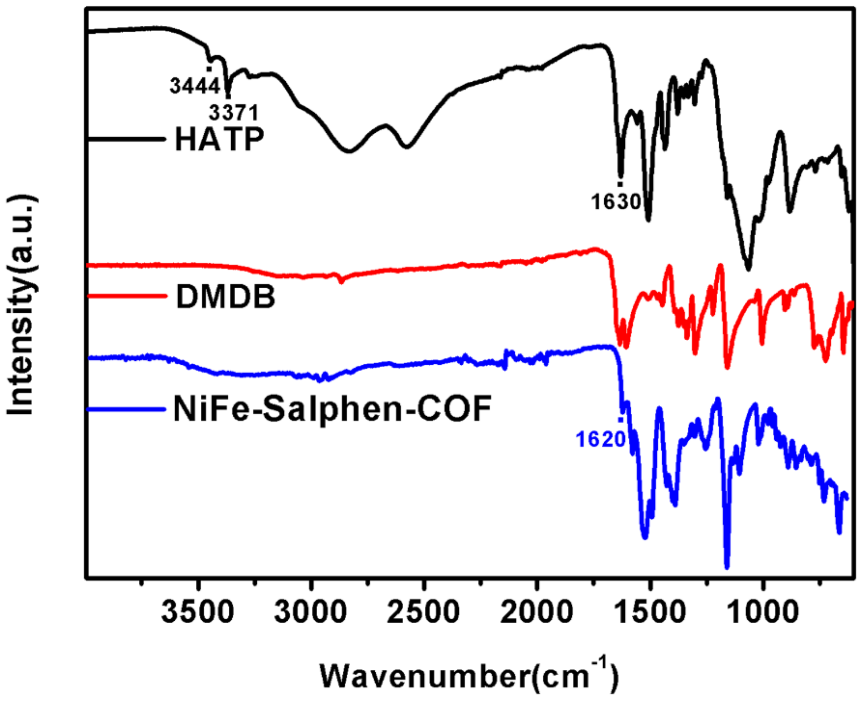

Fig. S19 FT-IR spectra of HATP, DMDB, and **NiFe-Salphen-COF**.

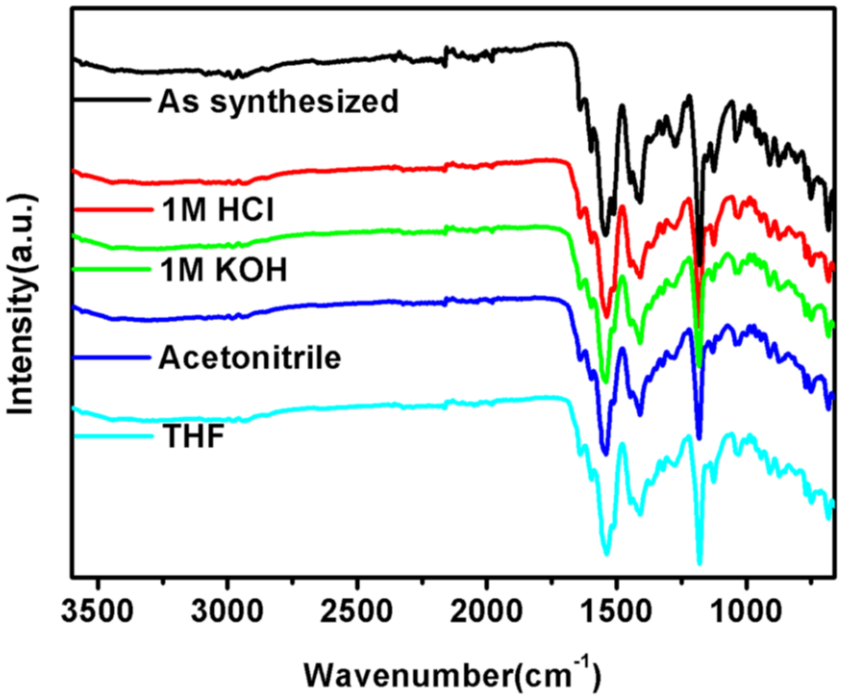

Fig. S20 FT-IR spectra of **NiFe-Salphen-COF** after treated in 1 M HCl, 1 M KOH and organic solvents for 3 days.

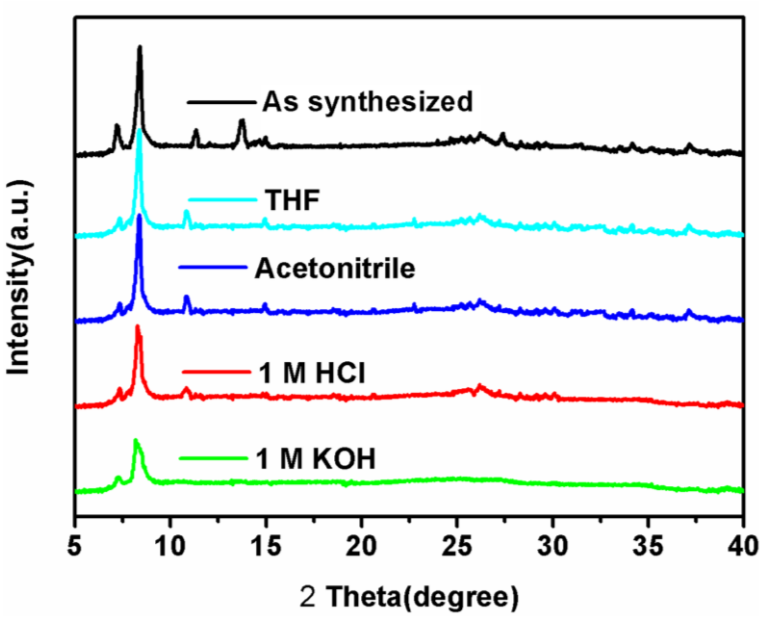

Fig. S21 PXRD patterns of **NiFe-Salphen-COF** after treated in 1 M HCl, 1 M KOH and organic solvents for 3 days.

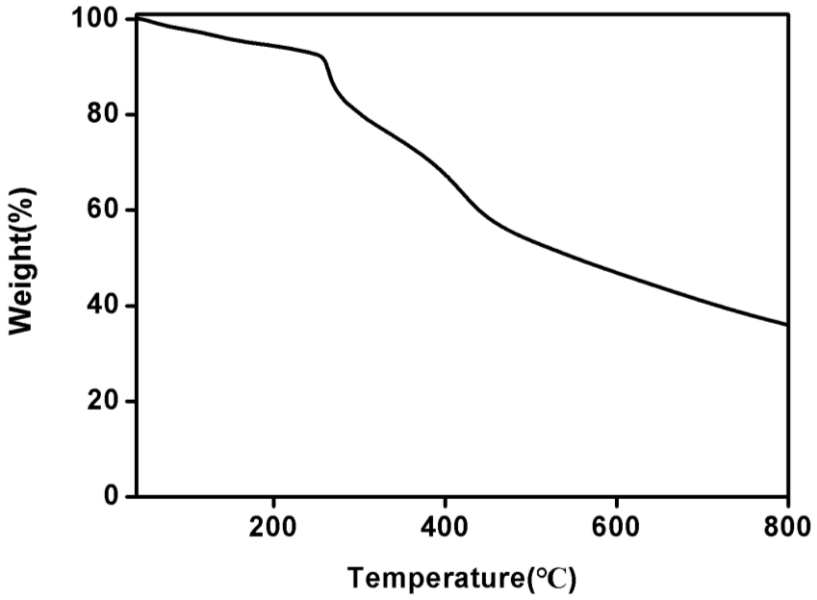

Fig. S22 Thermogravimetric analysis (TGA) curve of **NiFe-Salphen-COF**.

NiFe-Salphen-COF exhibited no discernible weight loss from 0 to 240 °C, and then started to decompose. At 800 °C, there was still 41% of weight residual. These indicate its good thermal stability.

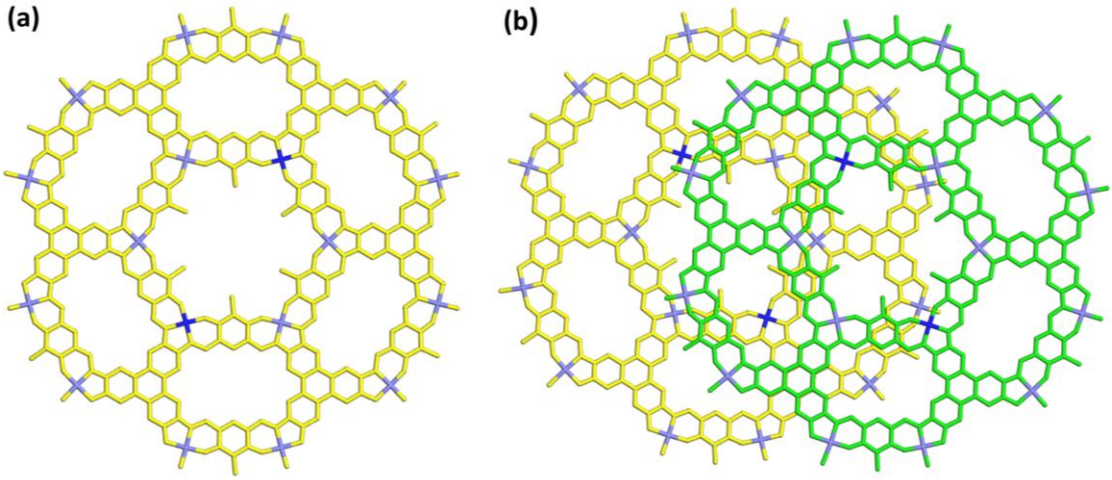

Fig. S23 (a) Eclipsed stacking AA model of **NiFe-Salphen-COF** (Purple : Ni, blue : Fe), (b) Staggered AB stacking of **NiFe-Salphen-COF** (Purple : Ni, blue : Fe).

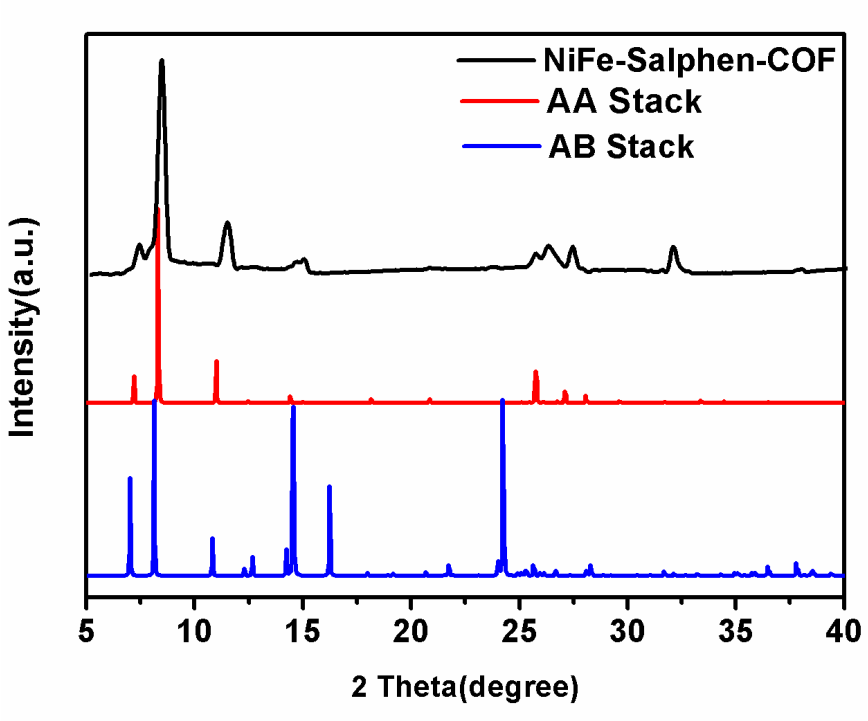

Fig. S24 PXRD patterns of **NiFe-Salphen-COF** (eclipsed AA stacking and Staggered AB stacking).

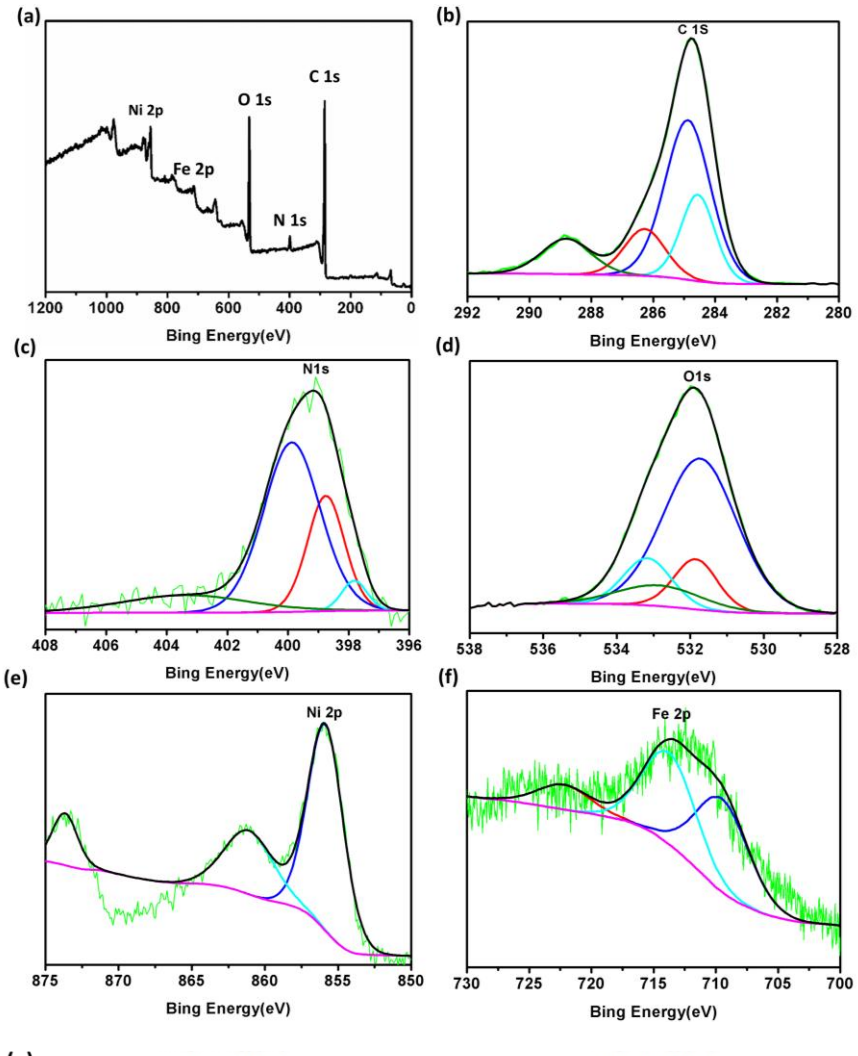

(g)

Elem.	NiFe-Salphen-COF at.-%
C	75.47
N	6.18
O	15.2
Ni	2.53
Fe	0.62

at.-%: atomic ratio in percentage.

Fig. S25 (a) Survey, (b) C 1s, (c) N 1s, (d) O 1s, (e) Ni 2p and (f) Fe 2p spectra of **NiFe-Salphen-COF**. (g) The elemental composition according to the XPS analysis.

The XPS survey of **NiFe-Salphen-COF** confirms the presence of C, N, O, Fe and Ni. The signals at 399.5 and 532.1 eV correspond to N 1s and O 1s, respectively. The Ni 2p spectrum exhibits two main peaks around 856.1 and 874.1 eV that are assigned to Ni $2p_{3/2}$ and Ni $2p_{1/2}$, respectively. The Fe 2p spectrum exhibits two main peaks around 713 and 722.5 eV that are assigned to Fe $2p_{3/2}$ and Fe $2p_{1/2}$, respectively.

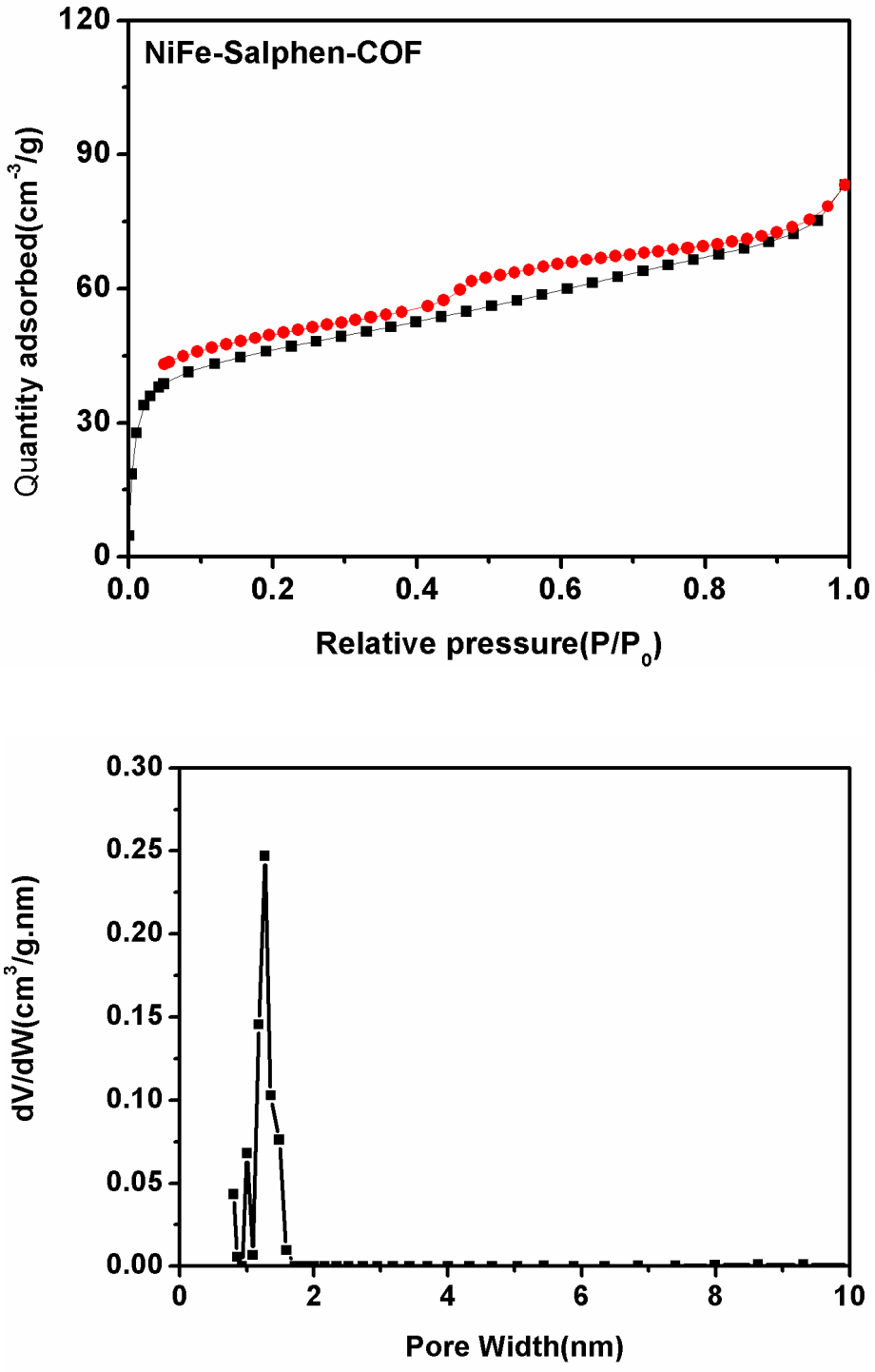

Fig. S26 N_2 adsorption/desorption isotherms of **NiFe-Salphen-COF** measured at 77.3 K. The BET surface area of **NiFe-Salphen-COF** was calculated to be 92 m^2 g^{-1}.

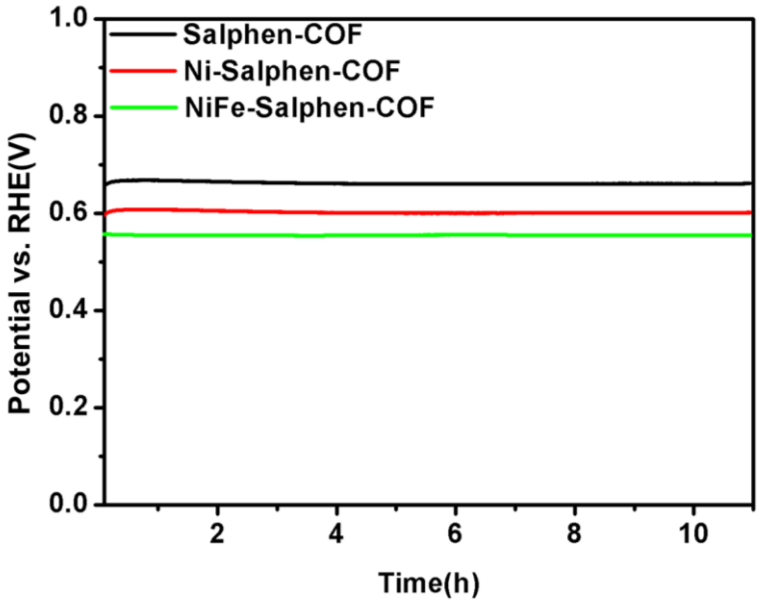

Fig. S27 Long-term stability test of the **Salphen-COF, Ni-Salphen-COF**, **NiFe-Salphen-COF** electrodes at a constant current density of 10 mA cm^{-2}.

Table S1 Fractional atomic coordinates for the unit cell of **Salphen-COF** with *P6* space group.

Salphen-COF			
P6 space group a = 24.5864 Å b = 24.5864 Å c = 3.4590 Å α = 90.0000° β = 90.0000° γ = 120.0000°			
C1	1.36454	1.03861	0.65904
C2	1.31597	1.06053	0.60161
C3	1.43326	1.09263	0.63798
O4	1.32459	1.10584	0.84444
C5	1.60216	1.32337	0.29077
C6	1.61264	1.26922	0.41221
C7	1.55777	1.20553	0.29254
C8	1.49584	1.19605	0.44206
C9	1.48358	1.24864	0.31948
C10	1.53891	1.31300	0.43034
N11	1.42474	1.23969	0.46627
N12	1.44364	1.13384	0.35005
O13	1.27860	1.17653	0.44146
C14	0.59577	0.72305	0.27137
C15	0.71135	0.76219	0.39468
C16	0.64250	0.71322	0.47979
C17	0.75700	0.75240	0.62044
C18	0.63148	0.64668	0.42160
C19	1.17480	1.20150	0.51836

Table S2 Fractional atomic coordinates for the unit cell of **Ni-Salphen-COF** with *P6* space group.

Ni-Salphen-COF			
P6 space group a = 24.5864 Å b = 24.5864 Å c = 3.4590 Å α = 90.0000° β = 90.0000° γ = 120.0000°			
Ni1	1.37734	1.18867	0.46813
C2	1.37140	1.05585	0.46813
C3	1.31508	1.05717	0.46813
C4	1.42955	1.10997	0.46813
O5	1.32374	1.11281	0.46813
C6	1.60925	1.33352	0.46813
C7	1.60925	1.27573	0.46813
C8	1.55161	1.21890	0.46813
C9	1.49516	1.21982	0.46813
C10	1.49516	1.27534	0.46813
C11	1.55161	1.33271	0.46813
N12	1.43744	1.26885	0.46813
N13	1.43744	1.16859	0.46813
O14	1.32374	1.21093	0.46813
C15	0.57045	0.68042	0.46813
C16	0.68492	0.74209	0.46813
C17	0.62860	0.68445	0.46813
C18	0.74358	0.74358	0.46813
C19	0.62868	0.62868	0.46813
C20	1.19585	1.19585	0.46813

Table S3 Fractional atomic coordinates for the unit cell of **NiFe-Salphen-COF** with *P1* space group.

NiFe-Salphen-COF			
P1 space group a = 24.6048 Å b = 24.6048 Å c = 3.6468 Å α = 79.3514° β = 79.3514° γ = 119.6345°			
Ni1	0.37719	0.18859	0.47166
C2	0.37142	0.05581	0.47166
C3	0.31506	0.05706	0.47166
C4	0.42954	0.10995	0.47166
O5	0.32355	0.11264	0.47166
C6	0.60923	0.33352	0.47166
C7	0.60923	0.27571	0.47166
C8	0.55157	0.21886	0.47166
C9	0.49510	0.21979	0.47166
C10	0.49510	0.27531	0.47166
C11	0.55157	0.33271	0.47166
N12	0.43736	0.26881	0.47166
N13	0.43736	0.16855	0.47166
O14	0.32355	0.21091	0.47166
C15	0.57046	0.68042	0.47166
C16	0.68494	0.74201	0.47166
C17	0.62858	0.68439	0.47166
C18	0.74362	0.74362	0.47166
C19	0.62860	0.62860	0.47166
C20	0.19809	0.19150	0.40103
Ni21	0.81141	0.18859	0.47166
C22	0.94419	0.31561	0.47166
C23	0.94294	0.25799	0.47166
C24	0.89005	0.31958	0.47166

O25	0.88736	0.21091	0.47166
C26	0.66648	0.27571	0.47166
C27	0.72429	0.33352	0.47166
C28	0.78114	0.33271	0.47166
C29	0.78021	0.27531	0.47166
C30	0.72469	0.21979	0.47166
C31	0.66729	0.21886	0.47166
N32	0.73119	0.16855	0.47166
N33	0.83145	0.26881	0.47166
O34	0.78909	0.11264	0.47166
C35	0.31958	0.89005	0.47166
C36	0.25799	0.94294	0.47166
C37	0.31561	0.94419	0.47166
C38	0.25638	0.00000	0.47166
C39	0.37140	0.00000	0.47166
C40	0.80850	0.00659	0.40103
Fe41	0.81141	0.62281	0.47166
C42	0.68439	0.62858	0.47166
C43	0.74201	0.68494	0.47166
C44	0.68042	0.57046	0.47166
O45	0.78909	0.67645	0.47166
C46	0.72429	0.39077	0.47166
C47	0.66648	0.39077	0.47166
C48	0.66729	0.44843	0.47166
C49	0.72469	0.50490	0.47166
C50	0.78021	0.50490	0.47166
C51	0.78114	0.44843	0.47166
N52	0.83145	0.56264	0.47166
N53	0.73119	0.56264	0.47166

O54	0.88736	0.67645	0.47166
C55	0.10995	0.42954	0.47166
C56	0.05706	0.31506	0.47166
C57	0.05581	0.37142	0.47166
C58	0.00000	0.25638	0.47166
C59	0.00000	0.37140	0.47166
C60	0.99341	0.80191	0.40103
Ni61	0.62281	0.81141	0.47166
C62	0.62858	0.94419	0.47166
C63	0.68494	0.94294	0.47166
C64	0.57046	0.89005	0.47166
O65	0.67645	0.88736	0.47166
C66	0.39077	0.66648	0.47166
C67	0.39077	0.72429	0.47166
C68	0.44843	0.78114	0.47166
C69	0.50490	0.78021	0.47166
C70	0.50490	0.72469	0.47166
C71	0.44843	0.66729	0.47166
N72	0.56264	0.73119	0.47166
N73	0.56264	0.83145	0.47166
O74	0.67645	0.78909	0.47166
C75	0.42954	0.31958	0.47166
C76	0.31506	0.25799	0.47166
C77	0.37142	0.31561	0.47166
C78	0.25638	0.25638	0.47166
C79	0.37140	0.37140	0.47166
C80	0.80191	0.80850	0.40103
Ni81	0.18859	0.81141	0.47166
C82	0.05581	0.68439	0.47166

C83	0.05706	0.74201	0.47166
C84	0.10995	0.68042	0.47166
O85	0.11264	0.78909	0.47166
C86	0.33352	0.72429	0.47166
C87	0.27571	0.66648	0.47166
C88	0.21886	0.66729	0.47166
C89	0.21979	0.72469	0.47166
C90	0.27531	0.78021	0.47166
C91	0.33271	0.78114	0.47166
N92	0.26881	0.83145	0.47166
N93	0.16855	0.73119	0.47166
O94	0.21091	0.88736	0.47166
C95	0.68042	0.10995	0.47166
C96	0.74201	0.05706	0.47166
C97	0.68439	0.05581	0.47166
C98	0.74362	0.00000	0.47166
C99	0.62860	0.00000	0.47166
C100	0.19150	0.99341	0.40103
Ni101	0.18859	0.37719	0.47166
C102	0.31561	0.37142	0.47166
C103	0.25799	0.31506	0.47166
C104	0.31958	0.42954	0.47166
O105	0.21091	0.32355	0.47166
C106	0.27571	0.60923	0.47166
C107	0.33352	0.60923	0.47166
C108	0.33271	0.55157	0.47166
C109	0.27531	0.49510	0.47166
C110	0.21979	0.49510	0.47166
C111	0.21886	0.55157	0.47166

N112	0.16855	0.43736	0.47166
N113	0.26881	0.43736	0.47166
O114	0.11264	0.32355	0.47166
C115	0.89005	0.57046	0.47166
C116	0.94294	0.68494	0.47166
C117	0.94419	0.62858	0.47166
C118	0.00000	0.74362	0.47166
C119	0.00000	0.62860	0.47166
C120	0.00659	0.19809	0.40103

Table S4 The water oxidation parameters of various porous organic polymers electrocatalysts.

POPs	Catalysts	Tafel slope (mV dec^{-1})	η_{10} (mV)	Ref.
COFs	Salphen-COF	138	354	This work
	Ni-Salphen-COF	72	284	This work
	NiFe-Salphen-COF	53	266	This work
	Co-TpBpy	59	510	1
	macro-TpBpy-Co	54	380	2
	Co-PDY	99	270	3
	$(CoP)_n$-MWCNTs	56	290	4
	CoNP-PTCOF	233	450	5
	PTCOF	290	600	5
	EPOP-700	76	297	6
	$Ni_{0.5}Fe_{0.5}$@COF-SO_3	83	308	7
	$Co_{0.5}V_{0.5}$@COF-SO_3	62	300	8
	COF-C_4N	64	349	9
	C_4-SHZ-COF	39	320	10
	FeNi-CoP-800	79	330	11
	$PSN_{0.4}$-CoNi/CNT-800	68	270	12
	CCoPTDP-FeNi-SiO_2	57	310	13
	IISERP-COF3-Ni_3N	79	230	14
CMPs	Co-POP	87	610	15
	Salen-CMP-Fe-1	93	318	16
	salen-CMP-Co-1	118	369	16
	Salen-CMP-Fe-2	80	267	16
MOFs	NNU-23	81.8	365	17
	CTGU-10c	58	240	18
	MAF-X27-OH	60	292	19

References

[1] H. B. Aiyappa, J. Thote, D. B. Shinde, R. Banerjee, S. Kurungot, *Chem. Mater.*, 2016, **28**, 4375-4379.

[2] X. Zhao, P. Pachfule, S. Li, T. Langenhahn, M. Ye, C. Schlesiger, S. Praetz, J. Schmidt, A. Thomas, *J. Am. Chem. Soc*., 2019, **141**, 6623-6630.

[3] H. Huang, F. M. Li, Y. Zhang and Y. Chen, *J. Mater. Chem. A*, 2019, **7**, 5575-5582.

[4] H. X. Jia, Z. J. Sun, D. C. Jiang and P. W. Du, *Chem. Mater.*, 2015, **27**, 4586-4593.

[5] J. H. Park, C. H. Lee, J. M. Ju, J. H. Lee, J. Seol, S. U. Lee and J. H. Kim, *Adv. Funct. Mater.*, 2021, **31**, 2101727.

[6] S. Gopi, K. Giribabu, M. Kathiresan, *ACS Omega.*, 2018, **3**, 6251-6258.

[7] Z. Gao, L. L. Gong, X. Q. He, X. M. Su, L. H. Xiao, F. Luo, *Inorg. Chem.*, 2020, **59**, 4995-5003.

[8] Z. Gao, Z. Yu, Y. Huang, X. He, X. Su, L. Xiao, Y. I. Yu, X. Huang, F. Luo, *J. Mater. Chem. A*, 2020, **8**, 5907-5912.

[9] C. Yang, Z. D. Yang, H. Dong, N. Sun, Y. Lu, F. M. Zhang, G. Zhang, *ACS Energy Lett.*, 2019, **4**, 2251-2258.

[10] S. Mondal, B. Mohanty, M. Nurhuda, S. Dalapati, R. Jana, M. Addicoat, A. Datta, B. K. Jena, A. Bhaumik, *ACS Catal.*, 2020, **10**, 5623-5630.

[11] Z. Liao, Y. Wang, Q. Wang, Y. Cheng, Z. Xiang, *Appl. Catal. B*, 2019, **243**, 204-211.

[12] D. D. Ma, C. Cao, X. Li, J. T. Cheng, L. L. Zhou, X. T. Wu, Q. L. Zhu, *Electrochim. Acta*, 2019, **321**, 134679.

[13] J. Guo, T. Li, Q. Wang, N. Zhang, Y. Cheng, Z. Xiang, *Nanoscale*, 2019, **11**, 211-218.

[14] G. Xu, H. Lei, G. Zhou, C. Zhang, L. Xie, W. Zhang, R. Cao, *Chem. Commun.*, 2019, **55**, 12647-12650.

[15] A. Singh, S. Roy, C. Das, D. Samanta, T. K. Maji, *Chem. Commun.*, 2018, **54**, 4465-4468.

[16]. W. Zhou, L. Yang, F. Y. Zhou, Q. W. Deng, X. Wang, D. Zhai, G. Q. Ren, K. L. Han, W. Q. Deng and L. Sun. *Chem. Eur. J*, 2020, **26**, 7720-7726.

[17] X. L. Wang, L. Z. Dong, M. Qiao, Y. J. Tang, J. Liu, Y. F. Li, S. L. Li, J. X. Su, Y. Q. Lan. *Angew. Chem. Int. Ed.*, 2018, **57**, 9660-9664.

[18] W. Zhou, D. D. Huang, Y. P. Wu, J. Zhao, T. Wu, J. Zhang, D. S. Li, C. H. Sun, P. Y. Feng, X. H. Bu, *Angew. Chem. Int. Ed.*, 2019, **58**, 4227-4231.

[19] X. F. Lu, P. Q. Liao, J. W. Wang, J. X. Wu, X. W. Chen, C. T. He, J. P. Zhang, G. R. Li, X. M. Chen, *J. Am. Chem. Soc.*, 2016, **138**, 8336-8339.